ChemComm

HIGHLIGHT

View Article Online
View Journal | View Issue

Cite this: *Chem. Commun.*, 2025, **61**, 18742

The metal–organic framework MIL-160: comprehensive insights into synthesis and applications

Mahdi Karimi *[a] and Christoph Janiak *[b]

Received 12th August 2025,
Accepted 3rd November 2025

DOI: 10.1039/d5cc04626b

rsc.li/chemcomm

This review offers a comprehensive analysis of MIL-160, a versatile aluminum-furandicarboxylate metal–organic framework (MOF) with significant applications across environmental, industrial, and biomedical fields. MIL-160's unique properties (high porosity, stability, and tailored channel structures) position it as a valuable material for gas separation, water harvesting, and energy storage. Various synthesis methods, including reflux, solvothermal, and dry-gel conversion methods, are examined for their effectiveness in optimizing MIL-160's structural and functional characteristics. The discussed applications range from atmospheric water capture and storage of greenhouse gases to biocatalysis and therapeutic delivery systems. The review highlights MIL-160's potential in high-impact applications, providing insights into future advancements in MOF design, especially for sustainable and energy-efficient technologies.

1 Introduction

Porous materials comprise solids with interconnected pore networks that present large internal surface areas for interactions with gases, vapors, and liquids, enabling capture, storage, separation, and catalysis.[1–5] Classical porous adsorbents (activated carbons, zeolites, silica gels, and clays) are of high importance in industry, yet are limited in tunability and selectivity for emerging process demands.[6,7] The advent of metal–organic frameworks (MOFs) expanded this landscape. MOFs are crystalline networks of metal nodes (ions or clusters) bridged by organic linkers, offering precisely adjustable pore sizes, shapes, and chemistries together with exceptionally high surface areas and modular functionality.[8] These attributes have translated into advances in gas capture and separation (*e.g.*, CO_2 and light hydrocarbons), catalysis, drug delivery, and water harvesting.[9–11]

Aluminum-based MOFs (Al-MOFs) have become especially attractive for practical deployment owing to the abundance, low cost, and benignity of aluminum, and because strong Al–O–carboxylate bonds frequently confer hydrothermal and chemical robustness under cycling.[12] Typical Al-MOF nodes are octahedral AlO_6 units (often $AlO_4(\mu\text{-}OH)_2$) connected *via* μ-OH bridges into corner-sharing chains that, with di- or tricarboxylate linkers, generate microporous frameworks with ~0.4–0.8 nm apertures. Importantly, many Al-MOFs can be synthesized through green and scalable routes,[13] including aqueous reflux, solvothermal methods at moderate temperature,[14] dry-gel conversion,[15] and even in continuous processes,[16] facilitating high space–time yields and straightforward shaping into pellets, granules, monoliths, or membranes for process integration.[17,18] The following Al-MOFs have the $AlO_4(\mu\text{-}OH)_2$ infinite or secondary building unit (IBU, SBU) and parallel one-dimensional square-to-rhombohedral-shaped channels and illustrate application-relevant behaviors: (i) ''wine-rack'' frameworks such as MIL-53(Al) exhibit breathing[19,20] and strong, reversible interactions with polar adsorbates;[21] (ii) isophthalate-based Al-MOFs (*e.g.*, CAU-10-H) and related materials show step-shaped water sorption suited to adsorption heat-transformation and atmospheric water harvesting;[22] and (iii) short-linker systems (*e.g.*, Al-fumarate) combine narrow windows with polar sites that benefit CO_2 and light-hydrocarbon separations.[23] Across these families, practical features—water/acid tolerance, low-temperature regeneration, and compatibility with composite formation—underpin their use in CO_2 capture and natural-gas conditioning, NH_3/SO_2 management, membranes for molecular sieving, and adsorption-based heating/cooling concepts.[24]

Within the broader MIL (Matériaux/Materials Institute Lavoisier) family, diverse frameworks are predominantly based on trivalent metals and di-/tricarboxylate linkers. MIL-160, first described by Cadiau *et al.* in 2015, stands out as an Al-MOF built from *cis*-μ-OH-bridged $\{AlO_6\}$ chains and the

[a] *Catalysts and Organic Synthesis Research Laboratory, Department of Chemistry, Iran University of Science and Technology, Tehran 16846-13114, Iran. E-mail: mahdi_karimi40@chem.iust.ac.ir, mahdikarimi1721@gmail.com*
[b] *Institut für Anorganische Chemie und Strukturchemie, Heinrich-Heine-Universität, D-40204 Düsseldorf, Germany. E-mail: janiak@hhu.de*

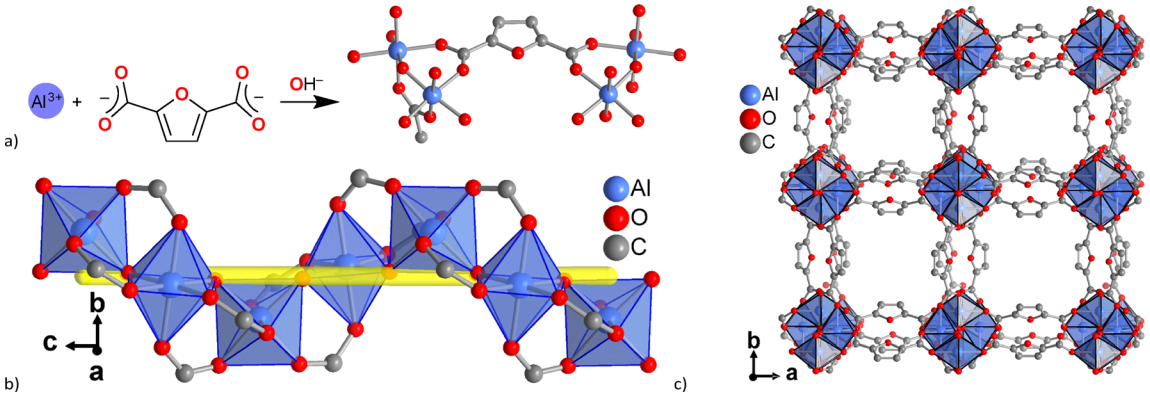

Fig. 1 Structural elements in the framework of MIL-160: (a) extended asymmetric unit with full aluminum coordination spheres and full linker bridging mode. (b) Section of the packing diagram with square-shaped one-dimensional channels along the crystallographic *c*-axis. (c) 4_1 Helical chains of *cis* OH-bridged [AlO_6] octahedra in polyhedral presentation (the yellow line indicates the 4_1 helical axis). Graphic produced by software Diamond[29] from the cif-file for MIL-160 (CSD-Refcode PIBZOS).[30]

2,5-furandicarboxylate (FDC) linker (Fig. 1).[25] 2,5-Furandicarboxylic acid is a bioderived ligand, starting from the biomass source fructose, so that the MOF MIL-160 can be considered a bio-derived material.[26,27] Its one-dimensional, square microporous channels and polar pore environment (μ-OH and furan O) provide strong, selective host–guest interactions that translate into promising behavior across water sorption/harvesting, adsorption heat transformation, acid/base gas capture (*e.g.*, NH_3 and SO_2), and small-molecule separations.[1,10,28]

Motivated by the practical attributes of Al-MOFs and by the distinctive performance and sustainability profile of MIL-160, including the use of a bio-derived linker and scalable aqueous/low-temperature syntheses, this review (i) surveys MIL-160's structure and physicochemical properties; (ii) compares synthesis routes (reflux, solvothermal, and dry-gel conversion) and shaping/composite strategies; and (iii) critically evaluates performance and mechanisms in water sorption/harvesting, adsorption-driven heat transformation, gas separation/storage (CO_2 and light hydrocarbons; NH_3/SO_2), and emerging bio-interfaces. We conclude with considerations for scale-up and cost, including techno-economic perspectives on bio-derived linker supply and industrial manufacturing.

2 Structure and physical properties

MIL-160 features a distinctive "wine-rack" structure characterized by square-shaped one-dimensional (1D) channels (Fig. 1). These channels, measuring approximately 4.0–7.0 Å in diameter, extend along the *c*-axis of the crystal, rendering the framework particularly suitable for gas storage and separation applications.[28,31] The structure comprises 4-fold helical chains of corner-sharing [$AlO_4(OH)_2$] octahedra, which are interconnected through *cis*-μ-OH bridges and through the bent or V-shaped organic linker FDC. This arrangement significantly contributes to the structural stability of MIL-160.[14,32]

The pore system of MIL-160 is crucial for its adsorption capabilities. Its relatively small pore size, combined with a functionalized surface adorned with μ-OH groups and heterocyclic furan oxygen centers, facilitates host–guest interactions with appropriate guests, making it selective for gas capture of NH_3,[23] and CH_4.[33] Furthermore, the presence of these functional groups increases the binding energy, leading to the preferred adsorption of molecules like C_2H_2F,[34] CO_2,[35] and SO_2.[36]

Additionally, MIL-160 boasts a resilient framework that is both thermally and chemically stable. It maintains its structural integrity over multiple cycles of adsorption and desorption of acidic or alkaline gases, an essential trait for industrial applications such as NH_3 capture and storage. The framework's capacity to undergo minor structural distortions during gas adsorption, particularly in the [AlO_6] moieties, further enhances its performance across various operational conditions.[23]

The pore size and specific surface area were determined using N_2 adsorption–desorption analysis, a standard technique for characterizing microporous and mesoporous materials. The Brunauer–Emmett–Teller (BET) surface area of MIL-160 has been reported to vary from 79 $m^2\ g^{-1}$ (with a total pore volume of 0.30 $cm^3\ g^{-1}$)[37] to 1200 $m^2\ g^{-1}$ (with a total pore volume of 0.40 $cm^3\ g^{-1}$),[38] depending on the material form and synthesis method (see below).[14] For instance, the powder form reaches 1150 $m^2\ g^{-1}$, while pellet versions measure around 1000 $m^2\ g^{-1}$.[39]

Synchrotron Rietveld refinements of MIL-160 were performed on three states: guest-free (dehydrated) MIL-160, hydrated MIL-160 containing ≈4 H_2O per framework formula unit, and N_2-loaded MIL-160 containing ≈2.3 N_2 per formula unit at 80 K. Hydration changes the space group from $I4_1/amd$ to $I4_1md$, whereas N_2 adsorption (80 K, up to 1 bar) and thermal cycling 80–400 K do not change the symmetry. In the N_2-loaded structure, the unit-cell volume increases from 4728 $Å^3$ (guest-free) to 4769 $Å^3$ (≈+0.9%). Refined pore metrics give a micropore volume (V_{mic}) of 0.404 $cm^3\ g^{-1}$. The shortest host–guest contact is μ-OH···N_2 = 2.983 ± 0.011 Å. Independent 77 K N_2 sorption reports S_{BET} = 1098 $m^2\ g^{-1}$ and V_{mic} (P/P_0 = 0.5) = 0.41 $cm^3\ g^{-1}$. In the hydrated model, water

oxygen atoms form an ice-like network, consistent with the composition $[Al(OH)(O_2C–C_4H_2O–CO_2)]\ 4H_2O$.[30]

3 Synthesis methods

The composition of MIL-160 includes FDC as the organic ligand and aluminum as the metal node. Various sources of aluminum are mentioned in the literature,[14] such as $AlCl_3\ 6H_2O$,[40] $Al(NO_3)_3{\cdot}9H_2O$,[37] and $Al(OH)(CH_3COO)_2$.[36] The synthesis of MIL-160 can be achieved through methods such as reflux,[41] solvothermal,[42] and dry-gel conversion[14] (Fig. 2).

3.1 Reflux method

The reflux method is commonly employed to synthesize MIL-160 and does not require hydrothermal conditions. For instance, Guo *et al.* utilized this synthesis method to prepare MIL-160 by reacting sodium hydroxide (NaOH), H_2FDC, water (H_2O), and aluminum chloride hexahydrate ($AlCl_3{\cdot}6H_2O$) under reflux at 378 K for 12 hours.[23] The resulting product had been collected through filtration, washed with dimethylformamide (DMF) and H_2O, and subjected to a 3-day solvent exchange with acetone. In MOF synthesis, washing with DMF is crucial for removing unreacted starting materials, by-products, or impurities, thereby ensuring a higher purity of the final product. While H_2O serves as the primary solvent, DMF effectively dissolves organic compounds and aids in achieving a more crystalline and purer MIL-160. The subsequent solvent exchange with acetone was necessary to eliminate residual solvents from the MOF pores, preparing the material for gas adsorption experiments. Acetone is particularly effective in preparing MOFs, such as MIL-160, for capturing and storing NH_3 without causing structural damage, thereby ensuring optimal performance in adsorption tests. NaOH deprotonates the organic linker, facilitating the coordination between aluminum ions and the linkers, which is essential for MOF formation.

Furthermore, after the acetone exchange, the material is activated to ensure complete desolvation before any gas adsorption measurements are taken. The acetone-exchanged MIL-160 is evacuated at 423 K under a dynamic vacuum of 1×10^{-6} mbar for 10 hours. This activation step effectively removes any residual guest molecules from the pores, yielding a fully desolvated, crystalline material that is ideally suited for subsequent gas adsorption experiments.[23]

3.2 Solvothermal method

The solvothermal method is often used for the synthesis of by reacting the precursors in a solvent at a temperature above its boiling point and autogeneous pressure to promote reaction and crystallization.[43] In their synthesis of MIL-160, Gu and coworkers used a solvothermal method starting with a biomass-derived H_2FDC solution that could contain its potassium salt (K_2FDC).[26] Aluminum nitrate nonahydrate $[Al(NO_3)_3{\cdot}9H_2O]$ was dissolved in the nitric-acid-treated H_2FDC solution inside a Teflon-lined container. The nitric acid helped dissolve any precipitated K_2FDC, which is poorly soluble, and ensured the solution's homogeneity. The mixture's pH was then adjusted to nearly neutral (7.4–7.7), a range crucial for the successful crystallization of MIL-160. The sealed container was heated for several hours, after which the white powder of MIL-160 was collected by centrifugation, washed multiple times with DMF and ethanol, and dried in a vacuum oven.[26]

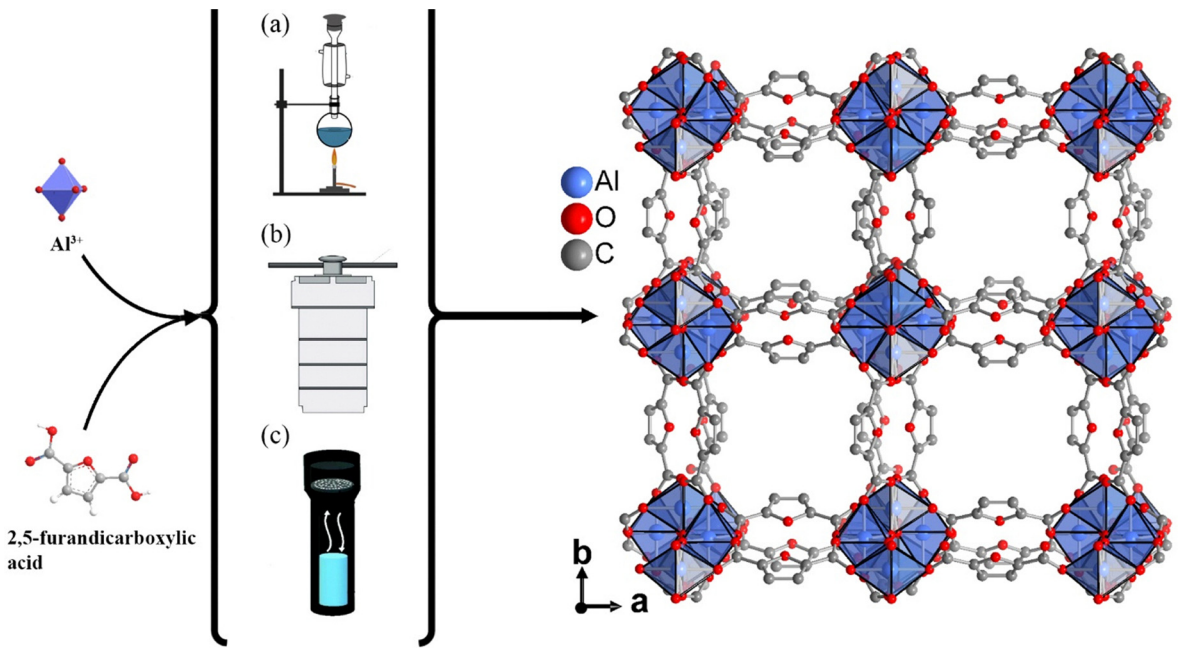

Fig. 2 Synthesis methods that have been used for the preparation of MIL-160: (a) reflux method,[23] (b) solvothermal method,[26] and (c) dry-gel conversion.[14]

3.3 Dry-gel conversion

The dry-gel conversion (DGC) method is an efficient approach for synthesizing MOFs while minimizing solvent use and waste generation. Unlike traditional solvothermal methods, DGC requires only enough solvent to wet the reactants, physically separating the solvent from the reaction mixture. This enables the recovery of largely uncontaminated solvents for reuse, significantly reducing waste production.[44] In a study by Tannert and coworkers, the DGC method was used to synthesize MIL-160 using aluminum salts, such as aluminum sulfate or aluminum chloride, along with H_2FDC. The reactants were ground and placed in a Teflon reactor on a sieve with H_2O or a H_2O/DMF mixture. The reaction proceeded at varying temperatures and times, yielding products that matched the BET surface area and pore volume of the materials obtained from the reflux method (Fig. 3(a)–(c)). This approach highlights the environmental advantages of DGC in producing MOFs with reduced ecological impact.[14]

In summary, the synthesis of MIL-160 is characterized by a diversity of methods and techniques. The reflux method and solvothermal method emerge as the most established synthesis approaches due to their reliability and adaptability. The dry-gel conversion method highlights a significant trend towards environmentally conscious practices by minimizing solvent waste.

Across the three routes used for MIL-160: reflux/solution, solvothermal, and DGC, the reported BET surface areas are broadly comparable: ~1070–1160 $m^2\ g^{-1}$ for solution syntheses and ~970–1180 $m^2\ g^{-1}$ for DGC. Solution/reflux routes typically show micropore/total pore volumes of ~0.41/0.45 $cm^3\ g^{-1}$. DGC uses only minimal solvent, reproducibly gives similar BET values but higher total pore volumes (~0.54–0.56 $cm^3\ g^{-1}$) owing to interparticle voids formed during gel conversion, and can exhibit

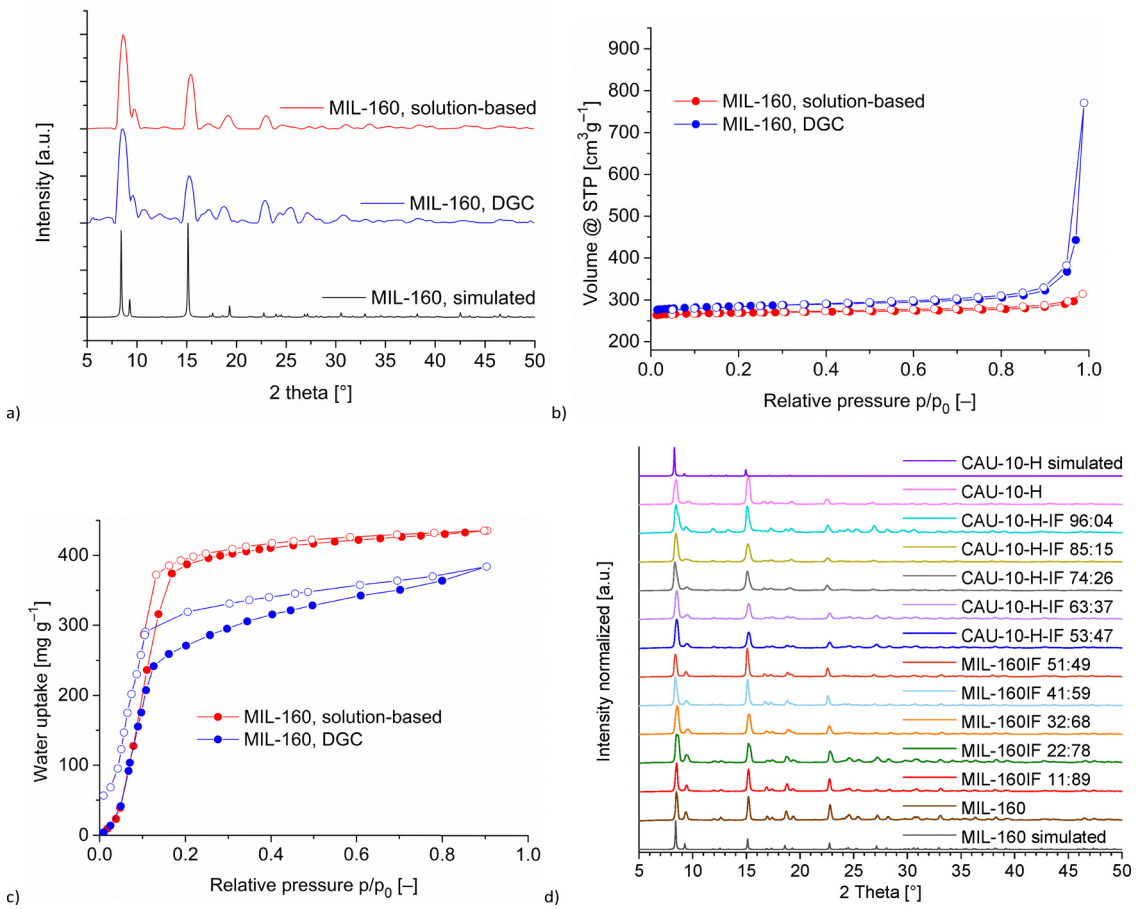

Fig. 3 Structural fingerprints and sorption behaviour of MIL-160 and related Al-MOFs. (a)–(c) MIL-160 was prepared by conventional solution synthesis *vs.* DGC. (a) PXRD patterns; the simulated MIL-160 diffractogram was calculated from the CSD structure PIBZOS. In the source work, the solution-synthesized sample matches the simulation more closely, whereas the DGC sample shows additional reflections. (b) N_2 adsorption–desorption isotherms at 77 K. The DGC material exhibits a steep uptake near $P/P_0 \gtrsim 0.9$, reflecting added interparticle meso-/macroporosity from gel-derived agglomeration and thus a higher total pore volume while preserving the intrinsic MIL-160 microporosity (c) H_2O adsorption–desorption isotherms at 20 °C. Filled symbols denote adsorption; open symbols denote desorption.[14] [reproduced from ref. 14 with permission from The Royal Society of Chemistry, copyright 2019]. (d) Mixed-linker series bridging CAU-10-H and MIL-160. PXRD patterns of MOFs synthesized with varying linker ratios of isophthalate (I) and furandicarboxylate (F), shown together with simulated patterns for MIL-160 (CSD: PIBZOS) and CAU-10-H (CSD: OQOBUT), highlighting the evolution of reflections as the framework composition shifts[46] [reproduced from ref. 46 with permission from The American Chemical Society, copyright 2019].

lower isolated yields (≈22–50%), whereas solution routes can reach higher isolated yields (≈55–93%).[14] Solvothermal growth is primarily used for *in situ* deposition on supports (*e.g.*, continuous MIL-160 membranes on α-Al_2O_3) without compromising crystallinity or textural properties. Scalable aqueous preparations under mild conditions (≈373 K, 24 h) have also been demonstrated.[26]

4 Structural and morphological control techniques

4.1 Mixed linker

The mixed-linker modification technique is employed in the synthesis of MOFs to tailor their properties by incorporating multiple organic ligands into the framework structure. This approach provides additional control over the pore environment, functionality, and overall performance of the MOF, making it highly adaptable for diverse applications.[45] A practical demonstration of this technique can be seen in the synthesis of mixed-linker aluminum-based MOFs by Schlüsener *et al.*,[46] where a solid-solution approach was employed to incorporate both isophthalate (IPA) and FDC as linkers, retaining the isoreticular MOF structures of CAU-10-H (with IPA) and MIL-160 (Fig. 3(d)). By varying the IPA-to-FDC ratio during synthesis, the hydrophilicity of the MOFs can be fine-tuned for cycling H_2O vapor sorption, such as in heat transformation applications. A higher coefficient of performance for the mixed-linker materials over MIL-160 illustrates the optimization potential for hydrophobicity/hydrophilicity under the exemplary calculation conditions. For compositions richer in FDC, the process employed a straightforward aqueous route, involving the reflux of $Al(OH)(CH_3COO)_2$ with the ligand mixture in H_2O for 24 hours. When the IPA content was higher than FDC, proportionate amounts of DMF were added to H_2O to ensure that the resulting MOF achieved crystallinity and porosity. This mixed-linker strategy highlights a versatile and efficient means to tailor MOF characteristics through simple adjustments of linker ratios alone.[46]

Fan *et al.* employed a mixed-linker strategy to fabricate a MIL-160/CAU-10-F MOF membrane with finely tuned pore apertures for enhanced gas separation.[47] By integrating MIL-160, which inherently exhibits a molecular sieving effect with a 5–6 Å pore size, with the highly polar, fluorine-functionalized CAU-10-F linker (featuring a 2.3 Å pore window), the team produced a continuous, well-intergrown membrane that combined the strengths of both frameworks. The resulting MIL-160/CAU-10-F membrane (which was fabricated on polydopamine (PDA) modified α-Al_2O_3 disks) demonstrated a stronger affinity for CO_2—driven by electrostatic interactions between CO_2 molecules and the electronegative O and F sites—leading to higher CO_2 binding energies (−38 kJ mol^{-1} compared to −35 kJ mol^{-1} of MIL-160), as well as a 11% increase in CO_2/CH_4 selectivity and a 31% boost in CO_2 permeability compared to the parent MIL-160 membrane. Moreover, its hydrophobic nature (water contact angle of 136.3°) confers superior resistance to H_2O vapor and hydrocarbons, making it particularly well suited for natural gas purification. This method also facilitated precise adjustment of the pore environment, optimizing the membrane for molecular sieving and rendering it more suitable for industrial gas separation applications.[47]

Luo *et al.* developed a two-linker MIL-160/Al-fumarate composite directly grown on chitosan-functionalized glass fiber paper (CGF) through an *in situ* synthesis process, aiming to harvest atmospheric water in arid climates.[48] The chitosan layer significantly enhanced MOF loading (306.71%) by improving electrostatic and hydrophilic interactions, allowing uniform growth of the mixed-linker MOFs on the CGF surface. By adjusting the fumaric acid (FA) to H_2FDC ratio, they optimized hydrophilicity and pore characteristics. The CGF-mixed-MOFs $(Al)_5$ (FA : H_2FDC = 5 : 5) achieved superior H_2O absorption—0.4 g g^{-1} at 30% RH, 0.3 g g^{-1} at 25% RH, and 0.3 g g^{-1} at 20% RH—compared to single-linker CGF-MIL-160(Al) (0.3, 0.2, and 0.2 g g^{-1}, respectively) and CGF-Al-fumarate (0.3, 0.1, and 0.1 g g^{-1}, respectively). The material retained crystallinity and structural integrity after 50 adsorption–desorption cycles, with an 87.5% H_2O release efficiency under simulated sunlight. This study shows how mixed-linker MOFs can be engineered for efficient and stable water harvesting in low-humidity environments.[48]

Building on these demonstrations, the linker opening angle dictates the μ-OH bridging topology along the infinite {Al(μ-OH)(O_2C–)} chains and, with it, whether two frameworks are isoreticular and can host a true solid-solution of linkers. As shown in Fig. 4, V-shaped FDC (≈117°) and IPA (≈120°) enforce *cis*-only AlO_6 connectivity, giving MIL-160 and CAU-10-H, respectively. Because they share the same *cis* chain SBU, partial substitution of FDC ↔ IPA is accommodated without changing the framework, hence mixed-linker solid solutions of MIL-160/CAU-10-H are feasible (Fig. 3(d)).

In contrast, TDC has a wider opening angle (≈150°) that stabilizes *cis*/*trans* (CAU-23) or even *trans*-only (MIL-53-TDC) Al–O chains. Mixing TDC with FDC therefore would combine incompatible SBUs (*cis*-only *vs. cis*/*trans* or *trans*). Under direct synthesis, this geometric mismatch resolves by nucleating separate crystallites, MIL-160 from FDC and CAU-23 (often with some MIL-53-TDC) from TDC, resulting in mixed-MOF phases rather than a single mixed-linker solid solution as for MIL-160 and CAU-10-H.[49]

4.2 Binder utilization and freeze casting

Shaping with a binder, such as silica, is a widely used technique to improve the mechanical stability and structure of MOFs, making them more practical for applications like catalysis or adsorption. In this process, a binder is incorporated into MOF powders to create materials with enhanced strength and integrity while preserving their porosity. Permyakova *et al*. utilized this approach to modify MIL-160. After synthesizing MIL-160 using a reflux method, the researchers mixed a specific amount of the MIL-160 powder with a silica sol solution as a binder. This mixture was processed using a pan-type granulator and wetted in a rotating fan to enhance the spherical shape of the

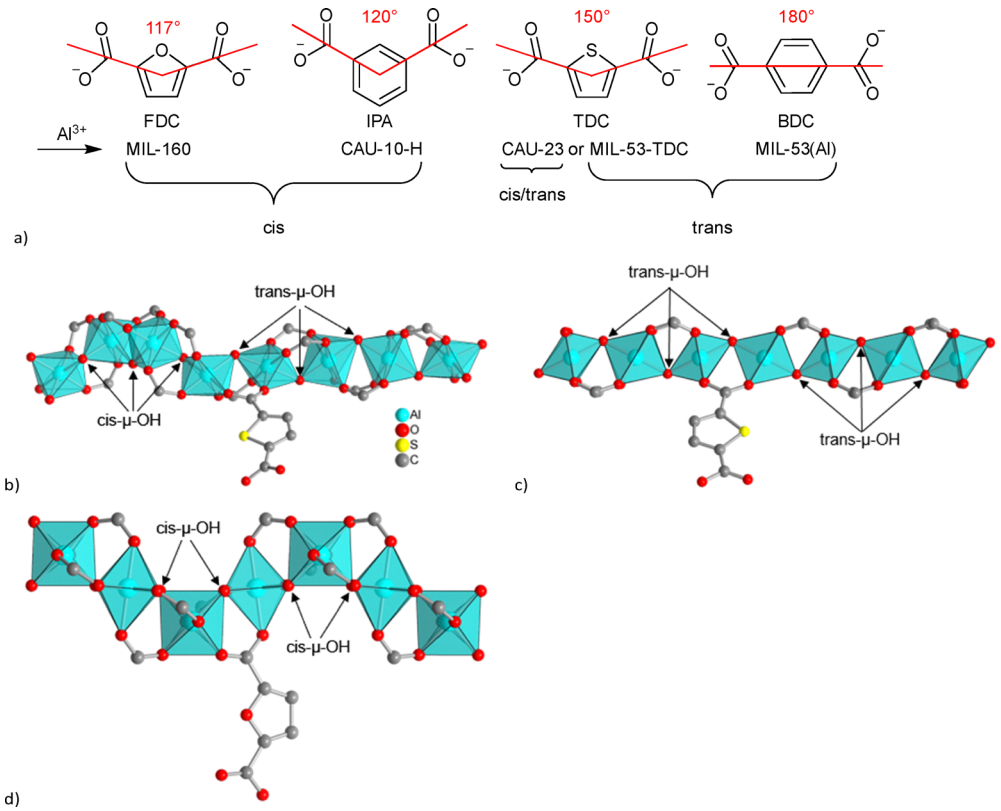

Fig. 4 (a) Schematic illustration of linker molecules relevant in this work, their opening angles, and the resulting Al-MOFs with their *cis*- and/or *trans*-μ-OH connectivity of the AlO_6 octahedra. (b) Illustration of Al–O chains of CAU-23 (*cis* and *trans*; helical and straight), (c) MIL-53-TDC (*trans*; straight), and (d) MIL-160 (*cis*; helical)[49] [reproduced from ref. 49 with permission from The Royal Society of Chemistry, copyright 2020].

granules. The resulting spheres were then dried. This shaping technique yielded spherical MIL-160 granules with improved mechanical stability, making them more suitable for industrial applications while retaining the intrinsic properties of the MOF (Fig. 5).[39]

Freeze-casting is a fabrication technique used to create porous materials through directional solidification. This method involves freezing a suspension and then allowing the solvent to sublime, leaving behind a solid structure with aligned pores.[51] It is particularly effective in modifying polymers to enhance their structural and functional properties. In a study by Hastürk and colleagues, freeze-casting of a MOF/polymer dispersion was employed to shape MIL-160 in a porous polymer binder.[52] The researchers dissolved a polymer, such as PVA, in H_2O, heated it, and added it to the activated MIL-160, stirring the mixture for several hours. The resulting suspension was placed into a syringe, frozen in liquid nitrogen, and subsequently warmed to allow the solidified monolith to be pressed out. The frozen MOF-polymer structure was then subjected to a dynamic vacuum, enhancing its porosity and structure.[52] In cases of MOF@PVA and MOF@PVP, water uptake was in good agreement with the MOF fraction and could be enhanced by the contribution of the hydrophilic polymer to the composite. The polymer PEI with MIL-160 resulted in MOF pore blocking.

Structural and morphological control techniques, such as mixed-linker modification, shaping with binders, and freeze-casting, underscore the growing emphasis on optimizing mechanical stability, porosity, and application-specific functionality. Among these, mixed-linker approaches show notable promise for industrial gas separation, while freeze-casting enhances structural and mechanical properties for advanced applications. Together, these methods exemplify the ongoing innovation and adaptability in the field of metal–organic framework synthesis, paving the way for the development of tailored materials with diverse industrial applications.

4.3 Membranes

Membrane separations often operate under milder conditions and can reduce energy use relative to distillation or cryogenic separation.[53] Unlike zeolites, many MOF membranes can be activated under vacuum at ~150 °C without burning structure-directing agents, mitigating crack-forming thermal stress. In Wu *et al.*,[42] "membrane" denotes a continuous MIL-160 layer grown *in situ* on a polydopamine (PDA)-modified α-Al_2O_3 disk for *p*-/*o*-/*m*-xylene separation by pervaporation. MIL-160's 1D channels (~0.5–0.6 nm) size-match *p*-xylene (PX, ~0.58 nm) while excluding *o*-/*m*-xylene (OX/MX, ~0.68 nm). Growth on PDA-modified supports (100 °C, 24 h) yields a dense, intergrown ~25 μm layer; without PDA, a continuous film does not form. At 75 °C, single-component fluxes reach PX = 486, OX = 10, MX = 12 g m^{-2} h^{-1} (ideal molar ratios PX/OX = 48.6; PX/MX = 40.5). For an equimolar PX/OX feed, PX flux is 467 g m^{-2} h^{-1} with a

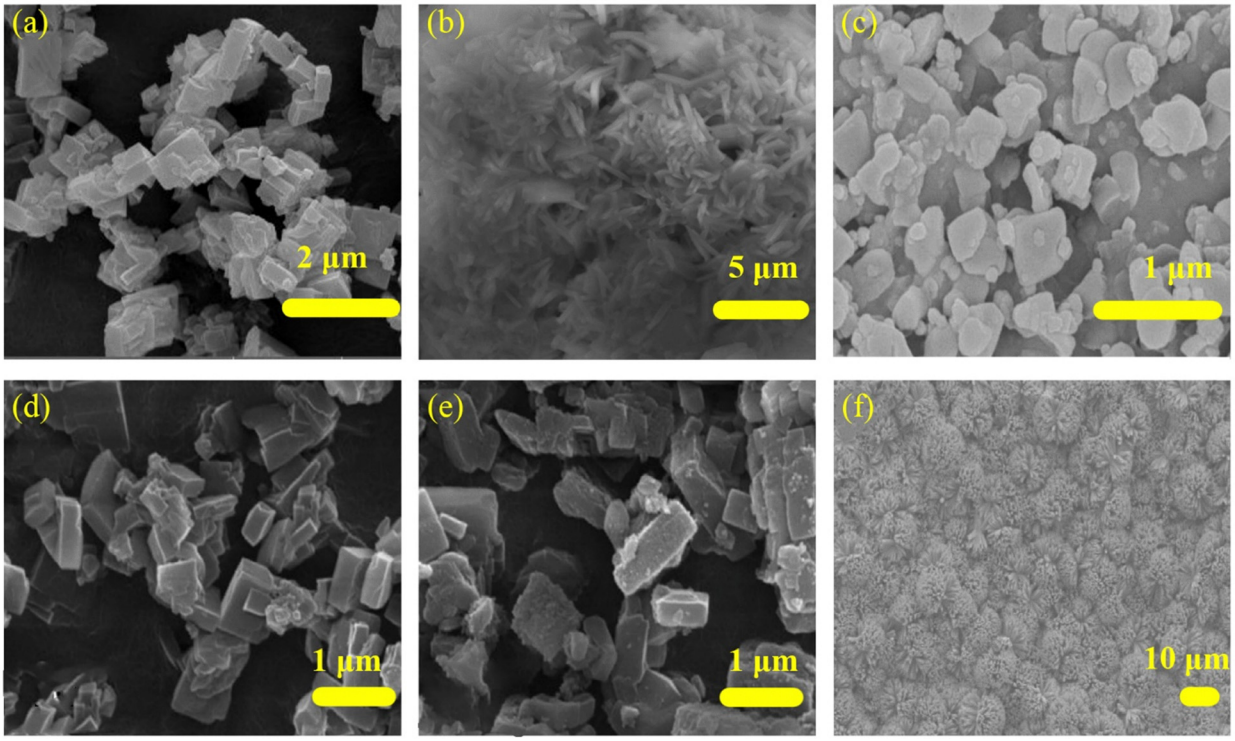

Fig. 5 FESEM images of MIL-160 with different synthesis methods (a), (b) hydrothermal method with two different morphologies [reproduced from ref. 38 with permission from Elsevier, copyright 2021] [reproduced from ref. 50 with permission from American Chemical Society, copyright 2023].[38,50] (c) Dry-gel conversion synthesis method [reproduced from ref. 28 with permission from Elsevier, copyright 2024].[28] (d), (e) Powder from the reflux method and then shaped with a silica binder [reproduced from ref. 39 with permission from Wiley, copyright 2017].[39] (f) Functionalized glass fiber paper loaded with two-linker metal–organic frameworks (CGF-mixed-MOFs(Al) (MIL-160 and Al-fumarate)) [reproduced from ref. 48 with permission from Elsevier, copyright 2022].[48]

separation factor of 38.5, comparable to MFI-zeolite pervaporation, and remains stable over 24 h with unchanged XRD/FESEM.

Mixed-gas simulations for MIL-160 (CO_2 with CH_4, SO_2, NO_2, or NO) show pressure- and composition-dependent behavior. For SO_2/CO_2, no CO_2 permeation is observed at 0.5 and 50 bar (consistent with SO_2-induced pore blocking), so the CO_2-relative selectivity is not quantifiable under these conditions. At 50 bars with 5 mol% CO_2, the steady-state composition within MIL-160 pores is ~20 mol% CO_2 for CH_4/CO_2 and NO/CO_2, ~16 mol% for NO_2/CO_2, and ~0.5 mol% for SO_2/CO_2, reflecting strong SO_2 affinity. Together with MIL-160's hydrothermal stability and prior PDA/Al_2O_3-supported MIL-160 PX/OX data (separation factor 38.5), these results indicate sub-100 °C size-sieving performance across liquid and gas separations.[54]

5 Techno-economic assessment and scale-up potential

Recent work by Severino *et al.* provides a detailed techno-economic evaluation of MIL-160 synthesis under green, aqueous, ambient-pressure conditions. Their pilot-scale process (30 L reactor, yield ≈93%, space-time yield ≈185 kg m^{-3} day^{-1}) demonstrated industrial feasibility and allowed for a full production-cost simulation. Estimated manufacturing costs decreased from ≈55 USD kg^{-1} at 100 t y^{-1} capacity to ≈30 USD kg^{-1} at 1000 t y^{-1}, with the bio-derived H_2FDC linker price emerging as the dominant factor. They concluded that costs below 10 USD kg^{-1} could be achievable as H_2FDC production scales up for bioplastics. Their results underscore that linker supply chains and process yields are the key levers toward affordable, large-scale MOF manufacturing.[27]

6 Applications

6.1 Water adsorption for heat transformation and water harvesting

MIL-160 exhibits water sorption properties, making it a candidate for water harvesting. Its adsorption isotherms are predominantly S-shaped (type V per IUPAC classification),[55] characterized by a steep increase in H_2O uptake within a specific relative humidity (RH) range, often around $P/P_0 \approx 0.3$. However, some studies note that uptake begins at a rate as low as 10% RH (Table 1). This S-shape is advantageous, enabling efficient water capture from low-humidity environments, such as arid climates. The maximum H_2O uptake varies slightly across studies, with values reported at approximately 0.38–0.4 g g^{-1} at 30 °C,[38,56] and up to four H_2O molecules per formula unit of the MIL-160 (≈0.4 g g^{-1}) at maximum capacity (Fig. 6(c) and (d)).[57] Its S-shaped uptake stems from the uniform pore structure (pore sizes ≈0.5–0.7 nm) and the capacity

Table 1 Structural information and water sorption properties of MIL-160

Inflection point of water sorption isotherm (P/P_0)	Max. water capacity (q_{max}) (g g^{-1}) (with its condition)	Pore size (d_{pore}) (nm)	Enthalpy of adsorption ($-\Delta_{ads}H$) (kJ mol^{-1})	Stability	BET surface area (m^2 g^{-1})	Pore volume (cm^3 g^{-1})	Synthesis method	Ref.
0.08	0.38 at 303.15 K (near saturation)	0.5	52–54 (zero loading)	High stability with no significant loss in performance over multiple cycles	~1200	0.4	Solvothermal	38
0.15	0.36 at P/P_0 = 0.90 (293 K)	—	54 (high loading)	—	1150	0.43–0.48	Reflux	46
—	0.364 (295.15 K)	—	—	—	—	—	Hydrothermal	57
—	—	0.4–0.6	56.6 (for H_2O vapor, average through loading)	Stable during water vapor exposure	1100–1200	0.45–0.50	Reflux	31
0.1–0.2	0.34 (max RH, 298.15 K)	—	—	—	789	0.30	Hydrothermal	37
—	0.252 at 15% RH, 298 K	0.57	69.6 (average through loading)	2.4% decrease after 10 cycles	—	—	Hydrothermal	58
~0.1	0.17/0.24/0.28 at 20/25/30% RH (700 min)	1.49	—	Good mass transfer efficiency and stability	840	0.31	Hydrothermal	48
—	0.231 (20% RH); 0.26 g g^{-1} (50% RH) (monolith)	0.7	62.4 (monolith), 72.3 kJ mol^{-1} (powder)(value at zero loading)	No significant loss over 50 cycles	1292	0.54	Dry-gel conversion	28
0.05	0.36 at P/P_0 = 0.50, 303 K	—	—	High hydrothermal stability	1162	0.45	Reflux	49
0.10–0.30	Powder ~0.39, pellet ~0.32 (reported near RH = 0.76).	—	—	Retains crystallinity and porosity after 1000 H_2O adsorption/desorption cycles	1122	0.46	Reflux	61
0.1	0.4 (293.15 K)	0.7	—	—	1070–1150	0.40–0.48	Reflux (dry-gel conversion)	14
0.08	0.4 (298 K)	—	Drops to 50 at 0.02 g g^{-1} (average through loading)	Reversible adsorption–desorption	1200	0.398	Reflux	56

from a substantial surface area (≈1200 m^2 g^{-1}),[56] fostering strong interactions between water molecules and hydrophilic functional groups, including hydroxyl, carboxylate, and furan ring oxygen atoms. MIL-160's minimal sorption hysteresis ensures nearly reversible adsorption–desorption cycles, while its regenerability at moderate temperatures (*e.g.*, 70–90 °C) enhances energy efficiency, which is critical for practical applications.[6,10,38,41]

Cadiau *et al.* (2015) first reported the water-sorption behavior of MIL-160. The water uptake began at $P/P_0 \approx 0.08$ (303 K), reached saturation by $P/P_0 \approx 0.18$ with ≈0.37 g g^{-1} capacity, and the material fully regenerated below 373 K.[25]

The application of MIL-160 in water-related technologies began gaining attention in 2019 with Schlüsener *et al.*'s[46] mixed-linker synthesis of isoreticular Al-MOFs [Al(OH)(IPA)$_a$(FDC)$_{1-a}$], which seamlessly spans the hydrophilicity range between CAU-10-H (a = 1) and MIL-160 (a = 0). As IPA content increases, the characteristic S-shaped water-adsorption isotherm shifts stepwise from an onset at $P/P_0 \approx 0.05$ for neat MIL-160 to $P/P_0 \approx 0.2$ for neat CAU-10-H, while total uptake remains above 300 mg g^{-1} at P/P_0 = 0.90 (293 K). Clausius–Clapeyron analysis of the isotherms at 293, 313, and 333 K shows that the isosteric heat of adsorption plateaus near 50–55 kJ mol^{-1} across all linker ratios, nearly matching water's latent heat and evidencing strong yet reversible sorption sites. Moreover, each mixed-linker MOF fully regenerates below 90 °C, underscoring their versatility for low-temperature desorption in cyclic water-harvesting and adsorption-heat-pump systems.[46]

Building on this initial work, a research study in 2020 provided deeper structural insights. Schlüsener *et al.*[49] advanced the understanding of MIL-160's water sorption by confirming its type V S-shaped isotherm, with uptake initiating at a low $P/P_0 \approx 0.05$, highlighting its high hydrophilicity. Achieving ≈0.4 g g^{-1} at 0.50 P/P_0 (303 K), the study contrasted MIL-160 with CAU-23, revealing distinct uptake profiles from a mixed-MOF composition due to the linker angle differences (FDC *vs.* TDC, *cf.* Fig. 4). This work underscored MIL-160's structural uniqueness, setting the stage for its specialized application in water capture.

Subsequently, in 2021, MIL-160's potential was more rigorously explored through mechanistic studies and practicalsystem development. Zu and Qin[38] detailed their S-shaped isotherms (max uptake 0.4 g g^{-1} at 30 °C) and modeled adsorption dynamics (intracrystalline diffusivity ≈1.0 × 10^{-11} m^2 s^{-1}, isosteric heat ≈53 kJ mol^{-1}), demonstrating superior cyclic performance over Zeolite 13X (for instance, at a regeneration temperature of 90 °C, MIL-160's capacity reaches approximately 105 kg m^{-3} compared to about 48 kg m^{-3} for Zeolite 13X). Concurrently, Silva *et al.*[31] optimized MIL-160 for a temperature swing adsorption (TSA) process, achieving 305 liters of H_2O per day per ton of adsorbent at 353 K. Its stability under humid conditions and minimal interference from CO_2, N_2, and O_2 affirmed its real-world viability.

Following these advancements, attention in 2022 turned towards detailed kinetic insights and the development of composite materials. Henry and Samokhvalov[57] used ATR-FTIR spectroscopy to quantify MIL-160's uptake (≈3.6 H_2O molecules/unit

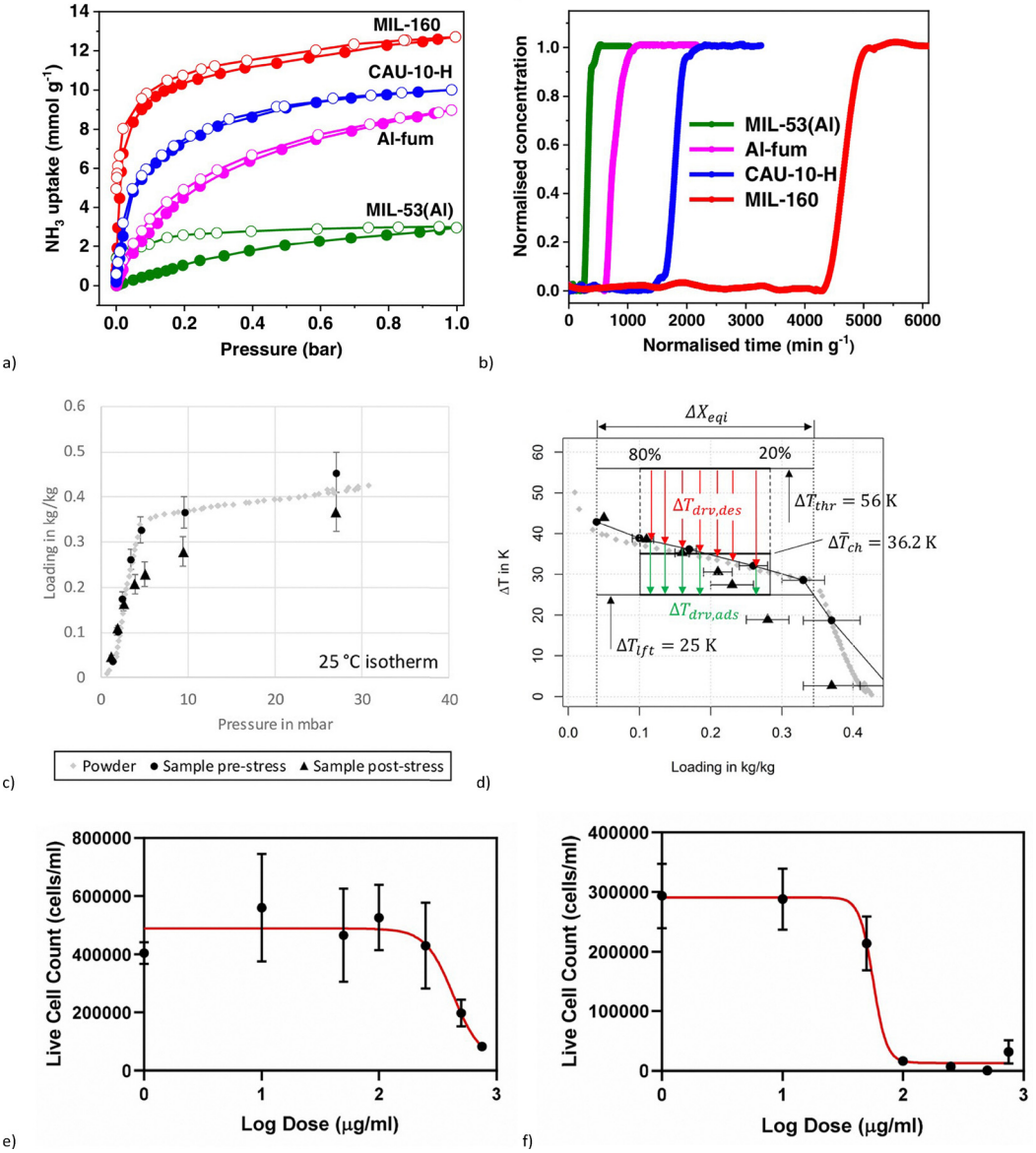

Fig. 6 Application-focused performance of MIL-160 compiled from representative studies. (a) Ammonia adsorption–desorption isotherms for MIL-160 at 298 K showing high- and low-pressure capacities of 12.8 and 4.8 mmol g^{-1} at 1.0 and 0.001 bar, respectively. (b) Dynamic fixed-bed breakthrough at 1000 ppm NH_3 (298 K) gives a 4.2 mmol g^{-1} dynamic uptake[23] [reproduced from ref. 23 with permission from *Nature*, copyright 2023]. (c) and (d) Device-relevant hydrothermal stress testing (≈70 000 temperature-swing cycles on binder-based coatings) indicates that MIL-160 undergoes an application-boundary-condition uptake decrease of ~35–45%, while degradation in heat/mass-transfer resistance is not observed for most tested MOFs (increase reported only for CAU-10-H)[59] [reproduced from ref. 59 with permission from Elsevier, copyright 2023]. (e) and (f) Human bronchial epithelial (BEAS-2B) dose–response (24 h) to MIL-160 (e) and ZIF-8 (f); four-parameter fits with mean ± SE, $n \geq 4$. Extracted IC_{50}: MIL-160 = 421 μg mL^{-1}, ZIF-8 = 57 μg mL^{-1} under identical conditions[60] [reproduced from ref. 60 with permission from Taylor and Francis, copyright 2019].

at 25% RH, maximal four), identifying five binding sites and pseudo-first-order kinetics (rate constant 0.01767 min^{-1}). Meanwhile, Luo *et al.*[48] developed a CGF-MIL-160 composite with an S-shaped isotherm (uptake at 10% RH, capacity 0.3 g g^{-1}), showcasing its adaptability in tailored adsorbents for low-humidity capture, despite a higher desorption temperature (71 °C).

Continuing the exploration of material enhancement, the year 2023 marked significant progress in hybridization strategies. Luo *et al.*[37] combined MIL-160 with MOF-303, yielding a physically mixed MOF with enhanced uptake (0.4 g g^{-1} at 30% RH), leveraging MIL-160's baseline properties (0.3 g g^{-1} at max RH) (Fig. 7(d) and (e)). In parallel, Li *et al.*[58] integrated MIL-160 into the porous polyacrylate material that has been chemically modified with amine ($-NH_2$) groups ($PAA-NH_2$) matrix, achieving 0.3 g g^{-1} at 15% RH with a low desorption energy (59 kJ mol^{-1}), demonstrating improved kinetics and stability over eight cycles, ideal for arid-region harvesting.

Finally, focusing on practical implementation and scalability in 2024, Yan *et al.*[28] introduced a low-temperature (60 °C) dry-gel

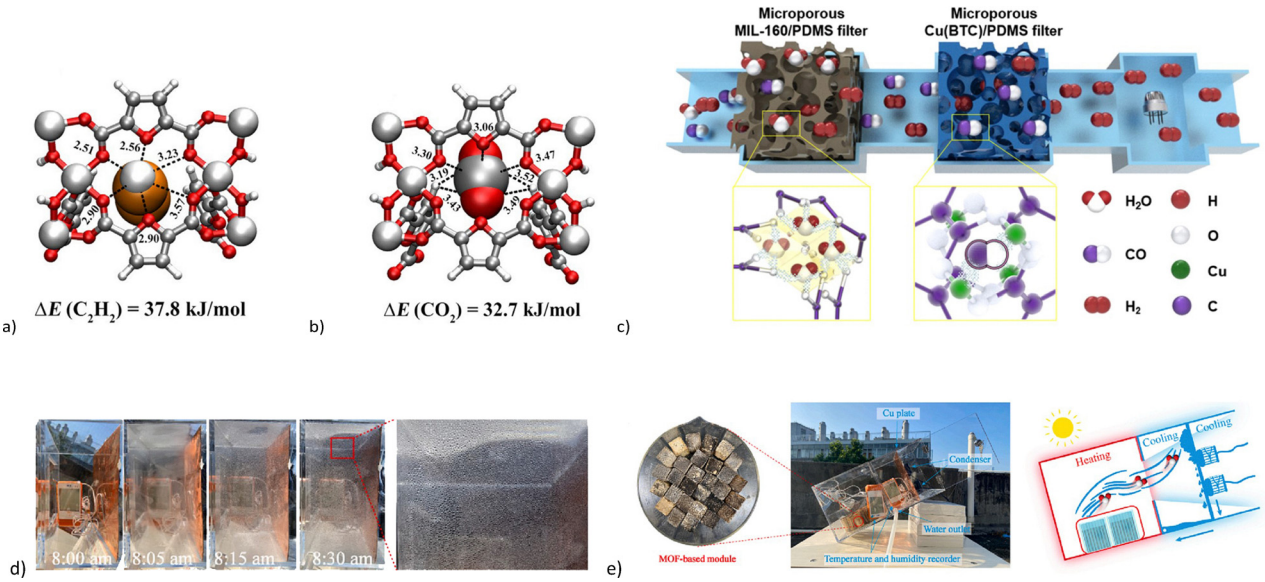

Fig. 7 (a) and (b) Canonical Monte Carlo (CMC) simulations modeled the primary binding sites for (a) C_2H_2 and (b) CO_2 in MIL-160. The distances are expressed in Å [reproduced from ref. 34 with permission from American Chemical Society, copyright 2022].[34] (c) A schematic representation of a filtration system utilizing a microporous elastomer filter coated with MOFs to enhance the selectivity for H_2 over CO while reducing the interference of moisture in metal oxide gas sensors. In a humid setting, when CO and H_2 are combined, H_2O molecules are filtered out by the microporous MIL-160/PDMS filter, while CO molecules are adsorbed by the microporous Cu(BTC)/PDMS filter, leading to a more selective and stable detection of H_2 in the air [reproduced from ref. 75 with permission from American Chemical Society, copyright 2020][75] (d) and (e) Outdoor operation of the MOF-based solar-driven water harvester under real sunlight. (d) Close-up image showing liquid water droplets condensed on the inner wall of the device's transparent enclosure during operation, indicating successful release and capture of moisture from the MOF material. (e) Photographs of the rooftop-installed water harvester: the left panel shows the MOF-based sorbent modules housed in the upper compartment during sunlight-driven desorption; the right panel shows condensed water droplets forming on the copper plate and inner surfaces of the lower condensation compartment, which are then collected at the bottom of the device [reproduced from ref. 37 with permission from Elsevier, copyright 2023].[37]

synthesis for MIL-160 powder and monoliths. This study reported a type I isotherm with rapid uptake at RH $<20\%$ (0.3 g g^{-1} powder, 0.2 g g^{-1} monolith at 20% RH). With a surface area of 1050–1210 m^2 g^{-1} and cycling stability over 50 cycles, this innovation significantly enhanced the scalability and practicality of MIL-160 for integration into water harvesting systems.

In conclusion, from its initial characterization in 2015 by Cadiau *et al.*[25] to advanced composites and scalable synthesis by 2024, MIL-160's evolution reflects a trajectory of increasing sophistication. Its S-shaped isotherms, high uptake, and energy-efficient regeneration have driven its progression from an adsorbent to practical water harvesting solutions, particularly for water-scarce regions.

6.2 Heat transformation technologies

MIL-160 is recognized as a highly versatile MOF with considerable potential in energy storage through heat transformation technologies. Its unique microporous structure allows for excellent H_2O sorption capabilities, making it suitable for various applications, including adsorption-based heating and cooling (see Section 5.1),[25,46] as well as seasonal energy storage. The studies reviewed indicate that MIL-160 demonstrates impressive energy storage potential, although the outcomes vary depending on specific applications and the environmental conditions involved.

Earlier, Permyakova *et al.* (2017)[62] highlighted that MIL-160 performs better when combined with $CaCl_2$ in composite form for seasonal heat storage applications. The MIL-160/$CaCl_2$ composite achieves impressive heat storage capacities of up to 310 kWh m^{-3}, proving effective for storing solar thermal energy during warmer months and utilizing it for heating in colder seasons. In the same year, Permyakova *et al.* (2017)[39] demonstrated that MIL-160 also shows particular promise for space heating applications, reaching an energy density of 343 Wh kg^{-1} with no degradation after 10 cycles. This stability, along with its scalability and eco-friendly synthesis, renders MIL-160 a strong candidate for long-term energy storage and redistribution solutions. More recently, Velte *et al.* (2023)[59] emphasized the role of MIL-160 in heat transformation systems, particularly in adsorption-based heating and cooling applications. However, they reported a 35–45% reduction in H_2O uptake after 70 000 hydrothermal cycles, indicating potential challenges with its long-term viability in continuous thermal cycling environments (Fig. 6(c) and (d)).

6.3 Gas separation and storage

MIL-160 has gained popularity due to its applications in gas separation, particularly in environmental and industrial contexts. Three recent studies highlight MIL-160's versatility in capturing and separating different gases: CO_2, NH_3, SO_2, CH_4, C_2 hydrocarbons (acetylene, C_2H_2 and ethane, C_2H_6), and propane, C_3H_6 (Table 2). Each study underscores different strengths of MIL-160's design and functionality, showing that

Table 2 Key properties of MOF-160 for gas separation

Pore size (d_{pore}) (nm)	BET surface area ($m^2\ g^{-1}$)	Gas separation	Capacity (mmol g^{-1}, 1 bar)	Enthalpy of adsorption ($-\Delta_{ads}H$) (kJ mol^{-1})	Selectivity	Synthesis method	Ref.
—	—	C_2H_2/CO_2, C_2H_2/C_2H_4	C_2H_2 = 11	—	—	Dry-gel conversion	64
0.7 (Horvath–Kawazoe (HK) cylinder model)	1138	C_2H_2/CO_2, *cf.* Fig. 7(a) and (b)	C_2H_2 = 9	C_2H_2 = 32 (zero loading) CO_2 = 27	10	Reflux	34
0.75 (non-local density functional theory (NLDFT) method)	1089	CH_4/N_2	CH_4 = 0.8	CH_4 = 24 (zero loading)	4	Hydrothermal	65
0.5–0.7 (HK)	1188	C_2H_6/CH_4, C_3H_8/CH_4	C_2H_6: 4.6, C_3H_8: 5.1	C_2H_6: 28, C_3H_8: 35 (zero loading)	C_2H_6/CH_4: 20, C_3H_8/CH_4: 174	Reflux	63
0.5 (geometric pore size)	1220	CO_2/N_2	CO_2 = 1 (0.15 bar)	CO_2 = −33 (zero loading)	34	Reflux	35
0.5–0.6 (geometric pore size)	—	CO_2/CH_4	CO_2	CO_2: −28.5, CH_4: −11 (zero loading)	—	Reflux	66
0.46, 0.98 (DFT model)	1134	– (focus on liquid phase)	—	—	m-NT/*p*-NT: 10, m-NT/*o*-NT: 6	Hydrothermal	67
0.5 (geometric pore size)	1170	SO_2/CO_2	SO_2 = 7	SO_2 = 42–55 (zero loading)	124–128	Reflux	36
0.4 to 0.6 (DFT model)	—	CO_2/N_2, CO_2/CH_4, CO_2/H_2, CO_2/CO	CO_2: 4	CO_2: 33, CH_4: 19, N_2: 17 (zero loading)	CO_2/N_2: 34, CO_2/CH_4: 8	Reflux	68
0.6 (method not clearly defined)	1130 (neat), 900 (granules)	—	2.3–8.9 (for VOCs)	—	—	Reflux	69
0.5–0.6 (geometric pore size)	986	CO_2/CH_4, CO_2/N_2	CO_2: 3, CH_4: 0.6, N_2: 0.1	CO_2: 32, CH_4: 11, N_2: 7 (near the zero-loading limit)	CO_2/N_2: 18, CO_2/CH_4: 4	Reflux	70
—	—	CO_2/N_2	CO_2: 2, N_2: 1	CO_2: 29, N_2: 7 (zero loading)	—	Reflux	71
—	1129	CO_2/CH_4, CO_2/N_2	—	—	CO_2/CH_4: 11, CO_2/N_2: 44	Solvothermal	72
0.55 (HK)	1000	NH_3	NH_3 = 13	NH_3 = 45–63 (increasing loading)	—	Reflux	23
0.55–0.58 (from argon sorption at 87 K)	1020	C_2H_6/CH_4	C_2H_6: 4, CH_4: 0.9	C_2H_6: 32, CH_4: 20 (zero loading)	C_2H_6/CH_4 = 10–30	Solvothermal	26
0.5–0.75 (HK)	1188	C_2H_2/C_2H_4, C_2H_6/C_2H_4	C_2H_6: 5, C_2H_2: 9	C_2H_2: 33, C_2H_6: 25, C_2H_4: 28 (zero loading)	C_2H_2/C_2H_4: 11, C_2H_6/C_2H_4: 2	Reflux	41
0.435 (method not clearly defined)	—	CO_2/CH_4	—	28 (zero loading)	CO_2/CH_4 = 71	Hydrothermal	47
0.47 (HK)	1104	CH_4/N_2	CH_4: 0.47 (298 K)	CH_4: 15 (coverage-dependent)	CH_4/N_2 = 5–9	Reflux	33
0.56 (from Ar adsorption isotherm at 87 K)	>1000	C_2H_6/C_2H_4	C_2H_6: 4.2–4.8, C_2H_4: 3.9–4.8	0.3 (C_2H_6/C_2H_4) (zero loading)	—	Reflux	50
0.5 (geometric pore size), 0.55 (HK)	1188	C_2H_2/CO_2	C_2H_2 = 7 (mmol cm^{-3})	C_2H_2: 35–36, CO_2: 31–32 (average through loading)	C_2H_2/CO_2 = 7	Reflux	26
0.5 (geometric pore size)	1108	SO_2/CO_2	SO_2 = 6	SO_2: 49, CO_2: 30 (zero loading)	SO_2/CO_2: 220	Reflux	73

its combination of high porosity, appropriate pore size, and high density of polar sites makes it a promising candidate across various gas separation applications (Fig. 7(a) and (b)). The study by Guo *et al.*[23] in the context of NH_3 capture, shows that MIL-160 can achieve impressive adsorption capacities due to its structural properties and multiple binding sites, including μ-OH groups and π-electron-rich furan rings, which facilitate strong host–guest interactions. These binding sites create a highly effective framework for NH_3 capture, achieving uptake capacities of 4.8 mmol g^{-1} at 0.001 bar and 12.8 mmol g^{-1} at 1.0 bar, making MIL-160 suitable for both high- and low-pressure NH_3 separation. Advanced techniques like neutron powder diffraction and infrared spectroscopy reveal structural changes upon NH_3 binding, indicating robust adsorption interactions that lead to selective and high-capacity NH_3 separation even under dynamic breakthrough conditions at low concentrations (1000 ppm). This makes MIL-160 a valuable solution for industrial and environmental remediation of NH_3 emissions (Fig. 6(a) and (b)).[23]

In another study, Xian *et al.*[41] evaluated MIL-160 for purifying ethylene (C_2H_4) streams by removing impurities such as C_2H_2 and C_2H_6, a critical task in the petrochemical industry. MIL-160 demonstrated a high C_2H_2 uptake of 9.1 mmol g^{-1} at 298 K, with a strong selectivity of 10.6 for C_2H_2 over C_2H_4. Density functional theory (DFT) calculations attributed this behavior to strong van der Waals and hydrogen-bonding interactions between the framework's oxygen heteroatoms and the C–H bonds of C_2H_2 and C_2H_6, resulting in higher binding energies compared to C_2H_4. Experiments confirmed that MIL-160 can efficiently separate a ternary mixture of C_2H_2, C_2H_4, and C_2H_6 in a single step, achieving polymer-grade C_2H_4 purity without additional purification steps. This performance highlights MIL-160's potential for petrochemical applications, where removing such impurities is essential for maintaining high-quality polymer production.[41]

Lastly, Xian *et al.*[63] conducted a study on natural gas upgrading that showcased MIL-160's ability to separate propane (C_3H_8) and ethane (C_2H_6) from CH_4, which is essential for both refining natural gas and recovering hydrocarbons for further industrial uses. MIL-160 demonstrated a C_3H_8 adsorption capacity of 5 mmol g^{-1} at 298 K and a notable capacity for C_2H_6 as well, even at low pressures. The framework's pore structure and high density of polar sites optimize interactions with C_3H_8 and C_2H_6 while reducing affinity for CH_4, making it highly selective and effective at low-pressure conditions. The MOF stability, confirmed through thermogravimetric and powder X-ray diffraction analyses, supports its performance under moist conditions and repeated adsorption cycles, addressing a key challenge for materials used in natural gas processing. Given the high costs and energy demands of traditional cryogenic distillation, MIL-160 offers a lower-energy alternative for hydrocarbon separation, with stable performance even after multiple regenerations.[63]

6.4 Bio-application

In the study by Chapman and Dinu (2023), the hydrophilic nature of MIL-160 was examined as a carrier for enzyme immobilization through physisorption on the outer MOF surface. Molecular dynamics simulations explored how MIL-160 interacts with enzymes such as carbonic anhydrase (CA) and myeloperoxidase (MPO), showing that stable binding is mainly driven by non-covalent interactions, especially hydrogen bonding. These interactions help maintain the structural integrity and active site accessibility of the enzymes, with CA retaining up to 72% of its catalytic activity when immobilized on MIL-160. This retention highlights the framework's potential for applications that require enzyme stability under synthetic conditions, including CO_2 sequestration with CA and antimicrobial strategies involving MPO. Compared to hydrophobic frameworks, the hydrophilic interface of MIL-160 is critical in preserving enzyme secondary structure and activity, thereby improving its usefulness in biocatalysis.[74]

A study by Wagner *et al.* examined the cytocompatibility and low toxicity profile of MIL-160 within a model of human lung epithelial cells (BEAS-2B). The findings underscore MIL-160's comparatively low cytotoxicity in relation to hydrophobic MOFs like ZIF-8, highlighting its viability in sensitive biomedical applications, including drug delivery and therapeutic methodologies. The study attributes its favorable interactions with biological systems to the material's stable and inert composition, positioning MIL-160 as a prudent material choice for applications necessitating biocompatibility with human tissues. These attributes reinforce its role in therapeutic delivery systems, where cellular safety is of utmost importance (Fig. 6(e) and (f)).[60]

Jansen *et al.* explored the use of MIL-160 in antifouling applications by integrating it with chitosan to form a composite that effectively resists microbial colonization in open environments. This composite leverages MIL-160's robust structural integrity and H_2O adsorption capacity, making it suitable for high-humidity environments such as dehumidification and water-harvesting systems. Coupled with the antifungal properties of chitosan, MIL-160 facilitates the development of a microbial-resistant surface, advantageous in applications that demand sustained material integrity over time. Collectively, these studies position MIL-160 as a promising MOF with extensive multifunctionality, suitable for a variety of biocatalytic, therapeutic, and environmental applications.[40]

Hwang *et al.* published a study focusing on enhancing semiconductor metal oxide (SMO) gas sensors, which are widely used due to their sensitivity and low cost but suffer from low selectivity and humidity interference. To address these issues, the authors coated a microporous polydimethylsiloxane (PDMS) filter with the two MOFs HKUST-1 (Cu (BTC)) and MIL-160. MIL-160 was applied specifically for moisture adsorption, leveraging its strong hydrophilic properties to reduce relative humidity around the sensor and improve gas selectivity by minimizing humidity-related interference (Fig. 7(c)).[75]

7 Future prospects and conclusions

The future of MIL-160 research presents exciting opportunities for broadening its applications across the energy, environmental,

and medical sectors. With advancements in synthesis techniques, tailored structural modifications could significantly enhance MIL-160's efficiency in gas separation, especially in renewable energy storage and greenhouse gas capture. Furthermore, investigating its water-harvesting capabilities under diverse humidity conditions may yield innovative solutions for arid regions. In the biomedical field, MIL-160's low cytotoxicity indicates its potential as a therapeutic delivery system. Future research that combines computational modeling with experimental approaches will be crucial in optimizing MIL-160's multifunctional properties, facilitating its adoption in sustainable and scalable technologies.

In conclusion, MIL-160 exhibits exceptional potential across various applications due to its unique structural, thermal, and chemical properties. This review highlights the versatile functionalities of MIL-160, emphasizing its capabilities in water harvesting, gas separation, and biomedical applications. The one-dimensional channel structure and high surface area, and stability enable MIL-160 to perform efficiently under diverse operational conditions. Its hydrophilic nature supports applications in atmospheric water capture, while the framework's compatibility with bio-derived ligands ensures safety in biocatalytic and therapeutic uses. Future research toward optimizing synthesis methods and enhancing MIL-160's stability in extreme environments could further expand its practical applications, particularly in sustainable resource conservation and environmental remediation technologies. As MIL-160 continues to be refined and explored, it is poised to become a foundational material in energy, environmental science, and healthcare.

Conflicts of interest

There are no conflicts to declare.

Data availability

No original data is included in this article.

References

1 J. Ferrando-Soria and A. Fernández, *Nano-Micro Lett.*, 2024, **16**, 88.
2 E. Jo, S. Yang, D. W. Kang and D. W. Kim, *Coord. Chem. Rev.*, 2024, **493**, 215958.
3 H. Zhong, Z. Wang, Y. Zhang, S. Suo, Y. Hong, L. Wang and Y. Gan, *Mater. Today Sustain.*, 2024, **26**, 100720.
4 Q. Ke, F. Xiong, G. Fang, J. Chen, X. Niu, P. Pan, G. Cui, H. Xing and H. Lu, *Adv. Mater.*, 2024, **36**, 2408416.
5 Y. Qian, B. Li, M. Irfan, D. Li and H. Jiang, *Coord. Chem. Rev.*, 2024, **518**, 216068.
6 C. Han, J. Yang, S. Dong, L. Ma, Q. Dai and J. Guo, *Sep. Purif. Technol.*, 2024, **354**, 128957.
7 N. Rangnekar, N. Mittal, B. Elyassi, J. Caro and M. Tsapatsis, *Chem. Soc. Rev.*, 2015, **44**, 7128–7154.
8 W.-L. Li, Q. Shuai and J. Yu, *Small*, 2024, **20**, 2402783.
9 X. Zhang, Y. Li and J.-R. Li, *Trends Chem.*, 2024, **6**, 22–36.
10 H. Gröger, A. Allahverdiyev, J. Yang and J. Stiehm, *Adv. Funct. Mater.*, 2024, **34**, 2304794.
11 Z. Han, M. Yuan, N. Nguyen, H.-C. Zhou, J. E. Hubbard and Y. Wang, *Coord. Chem. Rev.*, 2024, **514**, 215926.
12 Y. Hua, Y. Ahmadi and K.-H. Kim, *J. Hazard. Mater.*, 2023, **444**, 130422.
13 H. Reinsch, *Eur. J. Inorg. Chem.*, 2016, 4290–4299.
14 N. Tannert, C. Jansen, S. Nießing and C. Janiak, *Dalton Trans.*, 2019, **48**, 2967–2976.
15 N. Tannert, S. Gökpinar, E. Hastürk, S. Nießing and C. Janiak, *Dalton Trans.*, 2018, **47**, 9850–9860.
16 M. Rubio-Martinez, T. D. Hadley, M. P. Batten, K. Constanti-Carey, T. Barton, D. Marley, A. Mönch, K.-S. Lim and M. R. Hill, *ChemSusChem*, 2016, **9**, 938–941.
17 A. Samokhvalov, *Coord. Chem. Rev.*, 2018, **374**, 236–253.
18 E. Hastürk, C. Schlüsener, J. Quodbach, A. Schmitz and C. Janiak, *Microporous Mesoporous Mater.*, 2019, **280**, 277–287.
19 C. Serre, F. Millange, C. Thouvenot, M. Nogues, G. Marsolier, D. Louer and G. Férey, *J. Am. Chem. Soc.*, 2002, **124**, 13519–13526.
20 L. Alaerts, M. Maes, L. Giebeler, P. A. Jacobs, J. A. Martens, J. F. M. Denayer, C. E. A. Kirschhock and D. E. De Vos, *J. Am. Chem. Soc.*, 2008, **130**, 14170–14178.
21 S. Dhaka, R. Kumar, A. Deep, M. B. Kurade, S.-W. Ji and B.-H. Jeon, *Coord. Chem. Rev.*, 2019, **380**, 330–352.
22 D. Fröhlich, E. Pantatosaki, P. D. Kolokathis, K. Markey, H. Reinsch, M. Baumgartner, M. A. van der Veen, D. E. De Vos, N. Stock, G. K. Papadopoulos, S. K. Henninger and C. Janiak, *J. Mater. Chem. A*, 2016, **4**, 11859–11869.
23 L. Guo, J. Hurd, M. He, W. Lu, J. Li, D. Crawshaw, M. Fan, S. Sapchenko, Y. Chen, X. Zeng, M. Kippax-Jones, W. Huang, Z. Zhu, P. Manuel, M. D. Frogley, D. Lee, M. Schröder and S. Yang, *Commun. Chem.*, 2023, **6**, 55.
24 W. Fan, K.-Y. Wang, C. Welton, L. Feng, X. Wang, X. Liu, Y. Li, Z. Kang, H.-C. Zhou, R. Wang and D. Sun, *Coord. Chem. Rev.*, 2023, **489**, 215175.
25 A. Cadiau, J. S. Lee, D. Damasceno Borges, P. Fabry, T. Devic, M. T. Wharmby, C. Martineau, D. Foucher, F. Taulelle, C.-H. Jun, Y. K. Hwang, N. Stock, M. F. De Lange, F. Kapteijn, J. Gascon, G. Maurin, J.-S. Chang and C. Serre, *Adv. Mater.*, 2015, **27**, 4775–4780.
26 Y. M. Gu, H. F. Qi, S. Qadir, X. W. Liu, T. J. Sun, S. S. Zhao, Z. Lai and S. D. Wang, *ACS Sustainable Chem. Eng.*, 2021, **9**, 17310–17318.
27 M. I. Severino, E. Gkaniatsou, F. Nouar, M. L. Pinto and C. Serre, *Faraday Discuss.*, 2021, **231**, 326–341.
28 M. Yan, Z. Peng, W. Fu, B. Tan and Y. Luo, *Microporous Mesoporous Mater.*, 2024, **378**, 113256.
29 K. Brandenburg, *Diamond, Version 5.0.0; Crystal and Molecular Structure Visualization, Crystal Impact*, K. Brandenburg & H. Putz Gbr, Bonn, Germany, 1997.
30 M. Wahiduzzaman, D. Lenzen, G. Maurin, N. Stock and M. T. Wharmby, *Eur. J. Inorg. Chem.*, 2018, 3626–3632.
31 M. P. Silva, A. M. Ribeiro, C. G. Silva, I. B. R. Nogueira, K.-H. Cho, U.-H. Lee, J. L. Faria, J. L. Loureiro, J.-S. Chang, A. E. Rodrigues and A. Ferreira, *Adsorption*, 2021, **27**, 213–226.
32 Y.-M. Gu, H.-F. Qi, T.-T. Sun, X.-W. Liu, S. Qadir, T.-J. Sun, D.-F. Li, S.-S. Zhao, D. Fairen-Jiménez and S.-D. Wang, *Chem. Mater.*, 2022, **34**, 2708–2716.
33 Z. Huang, P. Hu, J. Liu, F. Shen, Y. Zhang, K. Chai, Y. Ying, C. Kang, Z. Zhang and H. Ji, *Sep. Purif. Technol.*, 2022, **286**, 120446.
34 Y. Ye, S. Xian, H. Cui, K. Tan, L. Gong, B. Liang, T. Pham, H. Pandey, R. Krishna, P. C. Lan, K. A. Forrest, B. Space, T. Thonhauser, J. Li and S. Ma, *J. Am. Chem. Soc.*, 2022, **144**, 1681–1689.
35 A. Henrotin, N. Heymans, M. E. Duprez, G. Mouchaham, C. Serre, D. Wong, R. Robinson, D. Mulrooney, J. Casaban and G. De Weireld, *Carbon Capture Sci. Technol.*, 2024, **12**, 100224.
36 P. Brandt, A. Nuhnen, M. Lange, J. Möllmer, O. Weingart and C. Janiak, *ACS Appl. Mater. Interfaces*, 2019, **11**, 17350–17358.
37 F. Luo, X. Liang, W.-C. Chen, S. Wang, X. Gao, Z. Zhang and Y. Fang, *Chem. Eng. J.*, 2023, **465**, 142891.
38 K. Zu and M. Qin, *Energy*, 2021, **228**, 120654.
39 A. Permyakova, O. Skrylnyk, E. Courbon, M. Affram, S. Wang, U.-H. Lee, A. H. Valekar, F. Nouar, G. Mouchaham, T. Devic, G. De Weireld, J.-S. Chang, N. Steunou, M. Frère and C. Serre, *ChemSusChem*, 2017, **10**, 1419–1426.
40 C. Jansen, N. M. Tran-Cong, C. Schlüsener, A. Schmitz, P. Proksch and C. Janiak, *Solids*, 2022, **3**, 35–54.
41 S. Xian, J. Peng, H. Pandey, W. Graham, L. Yu, H. Wang, K. Tan, T. Thonhauser and J. Li, *J. Mater. Chem. A*, 2023, **11**, 21401–21410.
42 X. Wu, W. Wei, J. Jiang, J. Caro and A. Huang, *Angew. Chem., Int. Ed.*, 2018, **57**, 15354–15358.
43 J. Hu, Z. Huang and Y. Liu, *Angew. Chem., Int. Ed.*, 2023, **62**, e202306999.

44 Z. Zhuang, Z. Mai, T. Wang and D. Liu, *Coord. Chem. Rev.*, 2020, **421**, 213461.
45 S. Bhattacharyya and T. K. Maji, *Coord. Chem. Rev.*, 2022, **469**, 214645.
46 C. Schlüsener, M. Xhinovci, S.-J. Ernst, A. Schmitz, N. Tannert and C. Janiak, *Chem. Mater.*, 2019, **31**, 4051–4062.
47 W. Fan, Y. Ying, S. B. Peh, H. Yuan, Z. Yang, Y. D. Yuan, D. Shi, X. Yu, C. Kang and D. Zhao, *J. Am. Chem. Soc.*, 2021, **143**, 17716–17723.
48 F. Luo, T. Liao, X. Liang, W.-C. Chen, H. Wang, X. Gao, Z. Zhang and Y. Fang, *J. Cleaner Prod.*, 2022, **373**, 133838.
49 C. Schlüsener, D. N. Jordan, M. Xhinovci, T. J. Matemb Ma Ntep, A. Schmitz, B. Giesen and C. Janiak, *Dalton Trans.*, 2020, **49**, 7373–7383.
50 K. H. Cho, J. W. Yoon, J. H. Lee, J. C. Kim, D. Jo, J. Park, S.-K. Lee, S. K. Kwak and U. Lee, *ACS Appl. Mater. Interfaces*, 2023, **15**, 30975–30984.
51 M. Li, X. Dai, M. Wang and H. Bai, *Small Methods*, 2024, **8**, 2300213.
52 E. Hastürk, S. P. Höfert, B. Topalli, C. Schlüsener and C. Janiak, *Microporous Mesoporous Mater.*, 2020, **295**, 109907.
53 D. S. Sholl and R. P. Lively, *Nature*, 2016, **532**, 453–457.
54 J. Chapman, N. Garapati, V. A. Glezakou, Y. Duan, J. Hu and C. Z. Dinu, *Mater. Adv.*, 2021, **2**, 5922–5934.
55 M. Thommes, K. Kaneko, A. V. Neimark, J. P. Olivier, F. Rodriguez-Reinoso, J. Rouquerol and K. S. W. Sing, *Pure Appl. Chem.*, 2015, **87**, 1051–1069.
56 S. Cui, A. Marandi, G. Lebourleux, M. Thimon, M. Bourdon, C. Chen, M. I. Severino, V. Steggles, F. Nouar and C. Serre, *Appl. Therm. Eng.*, 2019, **161**, 114135.
57 B. Henry and A. Samokhvalov, *Spectrochim. Acta, Part A*, 2022, **267**, 120550.
58 T. Li, H. Yu, J. Mi, C. Li, H. Meng and J. Jin, *Chem. Phys. Lett.*, 2023, **816**, 140391.
59 A. Velte, E. Laurenz and L. Rustam, *Appl. Therm. Eng.*, 2023, **227**, 120336.
60 A. Wagner, Q. Liu, O. L. Rose, A. Eden, A. Vijay, Y. Rojanasakul and C. Z. Dinu, *Int. J. Nanomed.*, 2019, **14**, 7583–7591.
61 S. Gökpinar, S. J. Ernst, E. Hastürk, M. Möllers, I. El Aita, R. Wiedey, N. Tannert, S. Nießing, S. Abdpour, A. Schmitz, J. Quodbach, G. Füldner, S. K. Henninger and C. Janiak, *Ind. Eng. Chem. Res.*, 2019, **58**, 21493–21503.
62 A. Permyakova, S. Wang, E. Courbon, F. Nouar, N. Heymans, P. D'Ans, N. Barrier, P. Billemont, G. De Weireld, N. Steunou, M. Frère and C. Serre, *J. Mater. Chem. A*, 2017, **5**, 12889–12898.
63 S. Xian, J. Peng, H. Pandey, T. Thonhauser, H. Wang and J. Li, *Engineering*, 2023, **23**, 56–63.
64 Z. Huang, K. Chai, C. Kang, R. Krishna and Z. Zhang, *Nano Res.*, 2023, **16**, 7742–7748.
65 Y. Yu, M. Shang, L. Kong, X. Li, L. Wang and T. Sun, *Chemosphere*, 2023, **321**, 138160.
66 M. Karimi, R. M. Siqueira, A. E. Rodrigues, F. Nouar, J. A. C. Silva, C. Serre and A. Ferreira, *Sep. Purif. Technol.*, 2024, **344**, 127260.
67 Y. Zhang, X. Huang, J. Huang, F. Lai, G. Huang, R. Lin, K. He, Q. Long, H. Ji and K. Chai, *Sep. Purif. Technol.*, 2025, **354**, 129062.
68 D. Damasceno Borges, P. Normand, A. Permiakova, R. Babarao, N. Heymans, D. S. Galvao, C. Serre, G. De Weireld and G. Maurin, *J. Phys. Chem. C*, 2017, **121**, 26822–26832.
69 C. Freitas, M. I. Severino, A. A. Mohtar, O. Kolmykov, V. Pimenta, F. Nouar, C. Serre and M. Pinto, *ACS Mater. Lett.*, 2024, **6**, 174–181.
70 M. Karimi, A. Ferreira, A. E. Rodrigues, F. Nouar, C. Serre and J. A. C. Silva, *Ind. Eng. Chem. Res.*, 2023, **62**, 5216–5229.
71 M. Karimi, R. M. Siqueira, A. E. Rodrigues, F. Nouar, J. A. C. Silva, C. Serre and A. F. P. Ferreira, *Ind. Eng. Chem. Res.*, 2024, **63**, 8772–8785.
72 D. Shade, B. Marszalek and K. S. Walton, *Adsorption*, 2021, **27**, 227–236.
73 J. X. Liu, J. Li, W. Q. Tao and Z. Li, *Fluid Phase Equilib.*, 2021, **536**, 112963.
74 J. Chapman and C. Zoica Dinu, *Langmuir*, 2023, **39**, 1750–1763.
75 K. Hwang, J. Ahn, I. Cho, K. Kang, K. Kim, J. Choi, K. Polychronopoulou and I. Park, *ACS Appl. Mater. Interfaces*, 2020, **12**, 13338–13347.